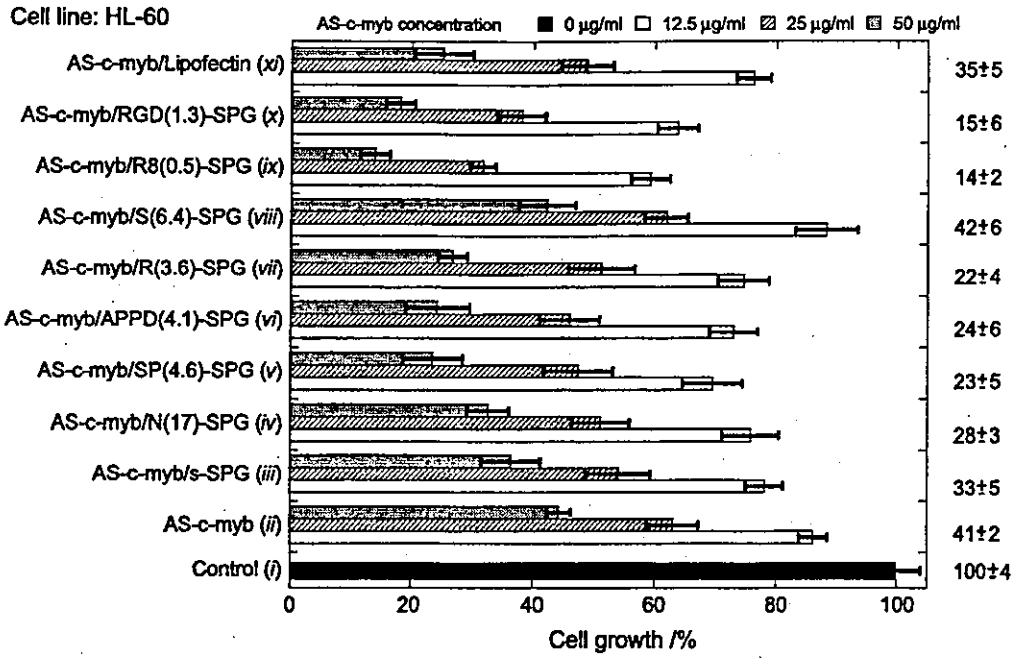

Fig. 8. Comparison of the cell growth for all samples, assayed with the HL-60 cell lines. The conditions were the exactly same as those in Fig. 5. The numerical results of the proliferation for 50 μg/ml dose are presented in the left side of the histograms.

myb, the cytotoxicity of this phosphorothioate sequence can be determined, which is about 14% at 50 μg/ml dose. Comparing with the naked S-c-myb system, the spermine and Lipofectin systems show lower growth than the naked system, indicating large cytotoxicity for these systems. The other systems are in the same level as the naked system. Fig. 7 examines the cytotoxicity of the carriers themselves. Here, the 150 μg/ml dose corresponds to the same amount of dose in weight as those in 50 μg/ml dose in Figs. 5 and 6. As expected, the unmodified s-SPG has little cytotoxicity. However, when we increased the modification level, the cytotoxicity became noticeable. Especially, spermine shows large cytotoxicity (see (vi) in the figure). More than that, Lipofectin is most toxic among the samples. These observations are consistent with results in Fig. 6.

3.3. Antisense effect in the leukemia cell lines; HL-60

Fig. 8 and Table 2 summarize the AS-c-myb antisense assay for the leukemia cell HL-60, when the assay was carried out in the exactly same manner as that of the A375 cell lines. Although the cell is different, the major trends are identical with those in A375. Similarly to A375, dramatic depression in the cell growth is observed for the R8(0.5)-SPG and RGD(1.3)-SPG systems (ix and x in Fig. 8). Since Table 2 shows negligibly small cytotoxicity for both systems, being in the same level as the unmodified s-SPG, the depressed cell growth should be mainly ascribed to the antisense effect. Their superiority can be ascribed to enhancement of endocytosis due to these functional peptides. From (v)–(vii) in Fig. 8, the modification by cations such as spermine depresses the cell growth considerably, so that it may seemingly induce the antisense effect. However, Table 2 shows that those modified s-SPG themselves (without AS-c-myb) reduce the cell growth considerably, indicating that these functional groups are more toxic for HL-60 than A375.

Table 2
Cytotoxicity for S-c-myb and the modified schizophyllan samples for the HL-60 cell lines

S-c-myb administration (50 μg/ml)	Cell growth (%)	Carrier administration (150 μg/ml)	Cell growth (%)
Control-2	100 ± 5	Control-3	100 ± 4
S-c-myb	95 ± 4		
S-c-myb/ s-SPG	96 ± 4	s-SPG	98 ± 5
S-c-myb/ N(17)-SPG	92 ± 4	N(17)-SPG	97 ± 6
S-c-myb/ P(4.6)-SPG	86 ± 6	SP(4.6)-SPG	89 ± 6
S-c-myb/ PPD(4.1)-SPG	87 ± 4	APPD(4.1)-SPG	89 ± 6
S-c-myb/ R(3.6)-SPG	91 ± 5	R(3.6)-SPG	96 ± 5
S-c-myb/ S(6.4)-SPG	92 ± 6	S(6.4)-SPG	95 ± 3
S-c-myb/ R8(0.5)-SPG	96 ± 5	R8(0.5)-SPG	97 ± 6
S-c-myb/ RGD(1.3)-SPG	96 ± 5	RGD(1.3)-SPG	97 ± 4
S-c-myb/ Lipofectin	76 ± 6	Lipofectin	81 ± 5

Cell line: HL-60.

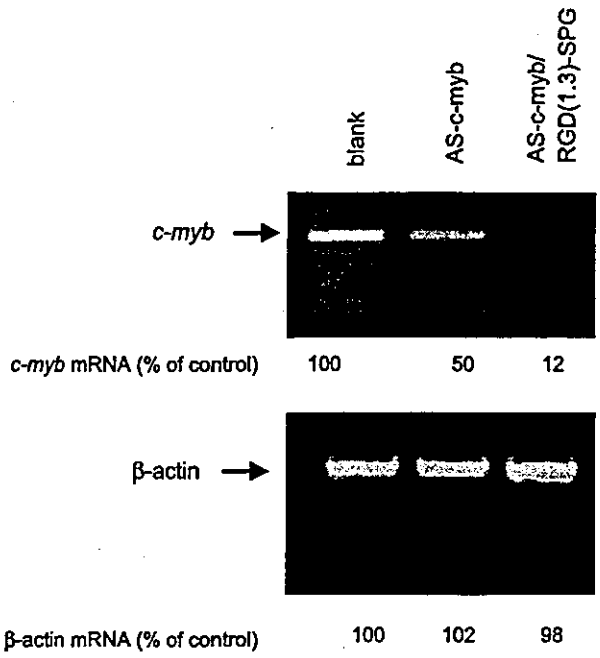

Fig. 9. Sequence-specific mRNA silencing confirmed by RT-PCR, comparing between naked ODN and its complex. A375 was treated with 60 μg/ml of AS ODN (targeting *c-myb* mRNA) or its RGD(1.3)-SPG complex. PCT products were resolved by agarose gel electrophoresis and visualized by GelStar®. Amplified DNA fragments were quantified by a gel documentation system (Alpha DigiDOC gel documentation system, Alpha Innotech). The numbers under the gel image indicate the relative intensity of the mRNA band to the reference.

Therefore, the reduced cell growth in (v)–(vii) in Fig. 8 is not related to the antisense effect, but to the cytotoxicity of these compounds.

3.4. Confirmation of the antisense effect by reverse transcriptase-mediated PCR (RT-PCR)

The enhanced anti-proliferation effect for AS-c-myb/s-SPG in Fig. 6 strongly supports that the antisense ODN depresses the *c-myb* expression. Encouraged by these results, we examined whether AS-c-myb (or its complex) silences the target mRNA in a sequence-specific manner, using RT-PCR. The results are presented in Fig. 9. As a reference, we evaluated the amount of the β-actin mRNA, comparing the control (no administration of ODN) with administration of AS-c-myb and AS-c-myb/RGD(1.3)-SPG. As shown in the lower panel in Fig. 9, there is no difference among the samples, indicating that administration of these ODN does not provide any effect on the amount of the β-actin mRNA. However, when we isolate the *c-myb* mRNA and evaluated the amount of mRNA by the same manner (the upper panel in the figure), the AS-c-myb and AS-c-myb/RGD(1.3)-SPG decrease the amount of mRNA, and the complex almost eliminated mRNA. These results evidence that AS ODN has silenced the target mRNA in a sequence-specific manner and the complex reduces the amount more drastically than the naked AS ODN, confirming that the antisense effect is enhanced in the complex system.

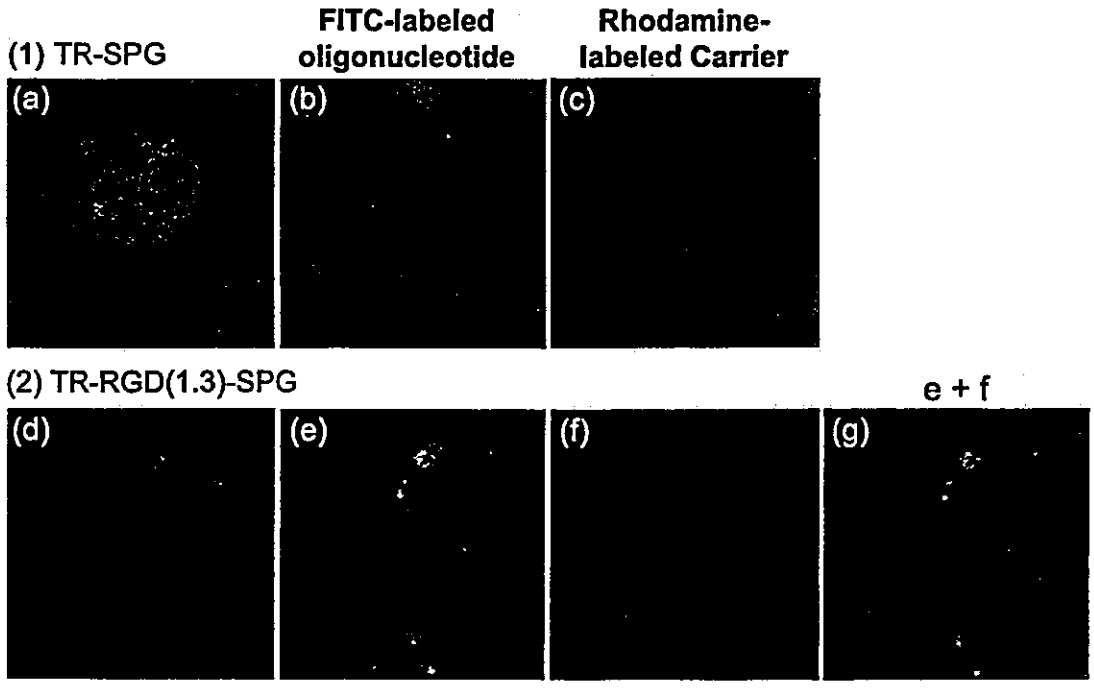

Fig. 10. Distribution of FITC labeled ODN and Rodamine labeled SPG in A375 measured with confocal fluorescent microscopy, comparing between the RGD-modified SPG (2) and unmodified one (1). The photos (b) and (e) are FITC fluorescence, (c) and (f) are corresponding Rodamine fluorescence, and (g) is a superimposed image of (e) and (f).

3.5. Cellular uptake observed by confocal fluorescent microscopy

To examine whether RGD(1.3)-SPG enhances cellular uptake of AS ODN, we exposed A375 cells to a complex made of TR-RGD(1.3)-SPG (Texas Red®-labeled RGD(1.3)-SPG) and 5′-FITC-labeled (dA_{50}) oligonucleotide and observed the cell morphology, comparing with that of the Texas Red®-labeled SPG complex (without RGD). Fig. 10 shows the typical confocal microscopic images. The photo (e) shows many bright green spots in the cell, while such a bright part is scarcely observed in the photo (b). Comparing between (e) and (f), the red color, namely the labeled SPG, is more condensed in the RGD complex than the reference. All results indicate the presence of RGD enhancing the uptake of ODN. It is interesting that there is clear difference in the distribution of the FITC-labeled ODN in the cell between (b) and (e). In panel (e), FITC-labeled (dA_{50}) seems to be located in the nucleus and vesicles more in than the other parts. This feature may be ascribed to difference in the ingestion mechanism.

4. Conclusion

The present report describes a unique chemical modification technique of schizophyllan, which enables us to introduce various functional groups only to the side chain. This technique consists of the periodate oxidation of the glucose side chain, followed by introduction of the functional groups into the formyl terminate. The introduced functional groups in this work were two α-amino acids (Arg and Ser), aminoethanol, spermine, *N,N′*-bis(3-aminopropyl)-1,3-propanediamine, octa-arginine(R8) and RGD. Using these modified s-SPGs as an AS ODN carrier, we conducted an in vitro antisense assay, administrating phosphorothioate AS ODN to the melanoma A375 or leukemia HL-60 cell lines to depress their *c-myb* mRNA. When we used the R8- or RGD-modified schizophyllan, the antisense effect was most enhanced among others. Their superiority can be ascribed to enhancement of internalization due to the specific action of these functional peptides. Furthermore, the cytotoxicity for these two modified schizophyllan derivatives was negligibly as small as the natural (unmodified) schizophyllan. One of the peculiar features of our system is that the complex is charged negatively in total, which is different from the conventional systems. We believe, therefore, that the present work provides a new approach to design a functional AS ODN carrier.

5. Materials and methods

5.1. Materials

Taito Co. Ltd. (Japan) kindly supplied the schizophyllan sample. The weight-average molecular weight (M_w) and the number of repeating units were found to be 1.5×10^5 and 231, respectively [19,20]. The ODN sequence of 5′-GTGCCGGGGTCTTCGGGC-3′ is well-known to bind to *c-myb* mRNA and lead depression of *c-myb* [41–46]. However, since short and hetero-ODNs cannot be combined with s-SPG [35,47], we had to attach a poly(dA) tail with 40 bases at the 3′ ends of this sequence. Thus, in this study, 5′-GTGCCGGGGTCTTCGGGC-$(dA)_{40}$-3′ phosphorothioate was used as an AS ODN and denoted by AS-c-myb. To examine whether the antisense effect really strives to suppress the cell growth, we use an ODN containing the sense sequence; 5′-CACGGCCCCA-GAAGCCCG-3′ as reference. For the same reason as the antisense sequence, the sense sequence was connected to the $(dA)_{40}$ tails at the 3′ ends and denoted by S-c-myb. Both AS-c-myb and S-c-myb were synthesized at Hokkaido System Science (Hokkaido, Japan) and purified with high-pressure liquid chromatography. The fetal bovine serum (FBS), and penicillin/streptomycin were purchased from Gibco/BRL. Dulbecco's modified Eagle's medium (DMEM®) and RPMI1640 were obtained from Nissui Pharmaceutical Co. Ltd. Bovine serum albumin (BSA) were obtained from Sigma.

Two peptides used in this work were chemically synthesized by 9-fluorenylmethyloxycarbonyl (Fmoc) solid-phase peptide synthesis on a Peptide Synthesizer ABI 433A, according to the established method [49]. Crude peptides were purified through reverse-phase HPLC (Hitachi LC system, elution: water/acetonitrile gradient) to afford pure S-peptide. The purified ones were identified with MALDI-TOF MS (PerSeptive Voyger PR) and the cald. $[M+H]^+ = 1371.65$ and obsed. = 1371.20 for H_2N-Cys-Arg-Arg-Arg-Arg-Arg-Arg-Arg-Arg-COOH, and $[M+H]^+ = 450.48$ and obsed. = 450.40 for H_2N-Cys-Arg-Gly-Asp-COOH. As the reagents for the peptide synthesis and its chemical modification, Fmoc-HN-Arg(Pbf)-Alko-PEG-resin, Fmoc-NH-Asp(tOBu)-Alko-PEG-resin, Fmoc-NH-Arg(pbf)-OH, Fmoc-NH-Gly-OH, Fmoc-Cys(Trt)-OH, DMF, *N*-methylpyrrolidone (NMP), piperidine, *O*-benzotriazoile-yl-*N,N,N′,N′*-tetramethyluronium hexafluorophosphate (HBTU), *N,N′*-diisopropylethylamine (DIPEA), 1,2-ethanedithiol (EDT), triisopropylsilane (TIPS), thioanisole and trimethylbromosilane (TMBS) were purchased from Watanabe Chemical (Japan). We also used *m*-cresol, TFA, DMSO, ammonia solution (28%) from Kishida Chemical, *t*-butylmetylether and phenol from Wako, and *N*-succinimidyl 3-maleimidopropionate from Tokyo Chemical Industry.

5.2. Chemical modification of the side chain of s-SPG

5.2.1. Method of the rout (I) in Fig. 3

The selective oxidation of the 1,2-diol group in the s-SPG side chain was carried out as described elsewhere [34]. The modification ratios of the aldehyde groups introduced were controlled by the amount of sodium

periodate ($NaIO_4$). After freezing-and-pumping followed by dialysis (fractionated molecular weight 1/4 12,000; Viskase), the s-SPG with the aldehyde side chain was obtained. The general procedure for introduction of α-amino acids (Arg and Ser), aminoethanol, spermine and *N,N'*-bis(3-aminopropyl)-1,3-propanediamine to s-SPG was as follows. The following method is for introduction of the α-amino acid, however, the basic procedure is the same for the other compounds.

K_2CO_3 (1.0 g) and oxidized s-SPG (0.1 g; 0.030 mmol/calculated aldehyde units) were mixed in dry DMSO. α-Amino acid methyl ester hydrochloride (3.0 mmol) were added to the DMSO solution and the resultant DMSO mixture was stirred under nitrogen at room temperature. After 2 days, an excess of $NaBH_4$ (0.3 g) was added and the mixture was stirred another 1 day. After quenching unreacted $NaBH_4$ with acetic acid, DMSO and inorganic materials were removed by dialysis under basic conditions. The ester group of the α-amino acid introduced was hydrolyzed to the corresponding acid during this process, because the ester IR peak at 1747 cm^{-1} (nujol) completely disappeared. Freezing-and-pumping of the resulting solution gave the α-amino acid-modified SPG. The percentage of α-amino acid introduced was determined by elemental analysis.

5.2.2. Method of the rout (II) in Fig. 3

The oxidized s-SPG (0.1 g; 0.005 mmol/calculated aldehyde units) were mixed in dry 10 ml DMSO. To the DMSO solution were added 10 ml ammonia solution (28%) and $NaBH_3CN$ 200 mg (excess), and the resultant DMSO mixture was stirred under nitrogen at room temperature. After lyophilization, the resultant solution gave the amine-modified s-SPG. Eighty milligrams of the amine-modified SPG dissolved in 10 ml of DMSO was added to 100 mg of *N*-succinimidyl-3-mareimidopropionate dissolved in 10 ml of DMSO and the mixture was stirred for 1 day at room temperature under nitrogen atmosphere. After the dialysis of the solution with distilled water, the solution was lyophilized. The white solid thus obtained was dissolved in 5 ml of DMSO and mixed with 50 mg of cystein-terminated peptide (6 eq. for maleimide). After the solution was stirred for 2 days at room temperature, the solution was repeatedly dialyzed with distilled water. Lyophilization of the resultant solution gave the peptide-modified s-SPG. The percentage of the peptide introduced was determined by elemental analysis.

5.3. Preparation of complex between ODN and s-SPG

Two milligrams of AS-c-myb were dissolved in 10 mM Tris buffer solution (pH 7.8) (1 ml). An appropriate concentration of modified s-SPG/DMSO solution was added to the AS-c-myb solution so that the water volume fraction was always adjusted to be 0.9 after mixing. In most cases, the molar ratio ($M_{s\text{-}SPG}/M_{ODN}$) was controlled to 1.5, where $M_{s\text{-}SPG}$ and M_{ODN} are the repeating molar concentration of s-SPG and AS-c-myb, respectively. After the AS-c-myb and s-SPG mixture was kept at 5 °C for one night to lead the complexation, DMSO was removed by ultrafiltration. After the filtration, the final concentration of AS-c-myb was determined by measuring the ultraviolet absorbance. To confirm the complexation between AS-c-myb and s-SPG, we measured the gel electrophoresis migration pattern. The details for these experiments are described in the preceding paper in the series of this work [20,29].

5.4. Cell culture

The melanoma cell: A375 and the leukemia cell: HL-60 (Promyelocytic leukemia, Human) were obtained from the American Type Culture Collection (ATCC, Rockville, MD). The A375 cells were maintained in DMEM® supplemented with 10% FBS. All medium contains a 1 wt.% penicillin/streptomycin mixture. The HL-60 cells were maintained RPMI 1640 and the other conditions were the same as those of the A375. The cell incubation was always carried out at 37 °C in fully humidified air containing 5 wt.% of CO_2.

5.5. Measurement of the cell proliferation

Cells were seeded in 96-well plates (Nunc) at a density of 2×10^4 cells/ml (1 well/100 μl) and allowed to attach to the plate overnight. The following day, the medium was changed with fresh medium and cells were treated with an appropriate amount of ODN (12.5, 25 and 50 μg/ml), ODN/s-SPG complex (containing 12.5, 25 and 50 μg/ml ODN), or modified or unmodified s-SPG (75, 150 μg/ml). Subsequently, cells were incubated for 3 days before measurement of the cell growth, because we already know that 3 days of incubation is long enough to give reliable results. The cell number was evaluated by the use of Cell Counting Kit-8® (Dojindo, Japan), called WST-8 assay. WST-8 assay uses a novel tetrazolium salt: 4-[3-(2-methoxy-4-nitrophenyl)-2-(4-nitrophenyl)-2H-5-tetrazolio]-1,3-benzene disulfonate sodium salt (WST-8), which produces a water-soluble formazan dye upon reduction mediated by dehydrogenase in the living cells [32]. After incubation for 3 days, 10 μl of the Cell Counting Kit-8 working solution (containing WST-8 and 1-methoxy-5-methylphenazinium methosulfate) was added to each well, and incubated for 4 h at 37 °C for A375 and for 8 h at 37 °C for HL-60. Plates were read on microplate reader Multiskan JX (Thermo Labsystems) using a wavelength of 450 nm in comparison with 650 nm. Each control or treated cells was tested in triplicate wells, and the mean and standard deviation of the values was plotted. All growth studies were carried out at least twice.

5.6. RT-PCR

RT-PCR was carried out to observe sequence-specific silencing of mRNA [50]. A375 cells were plated in 24-well plates (Nunc) at an initial concentration of 2×10^4 cells/ml in medium, and allowed to attach to the plate for overnight. The following day, the cells were treated with 60 μg/ml AS ODN or the RGD complex. After 2 days, the cells were harvested with 0.25% trypsin-EDTA in PBS. Total RNA was isolated with RNeasy Mini Kit (QIAGEN) as recommended by the manufacturer. RT-PCR was performed with ThermoScript RT-PCR system (Invitrogen). In a PCR tube were added RNA (0.9 μg), oligo(dT) primer, dNTPs (10 mM, 2 μl), DTT (0.1 M, 1 μl), and RNaseOUT (2 U/μl), Thermoscript RT (0.75 U/μl). Synthesis of the first-strand cDNA was done at 55 °C for 40 min in DNA thermal cycler (T gradient, Biometra, Germany). The resulting cDNA fragments were amplified with 2 U/ml of *Taq* polymerase, $MgCl_2$ (50 mM, 1.6 μl), and dNTPs (10 μM, 1 μl), 15 pmol of each primer. Reagents were purchased from Invitrogen. Thermal cycling consists of 1 min denaturing at 95 °C, 1 min annealing at 55 °C (*c-myb*) or 57 °C (β-actin), and 1 min extension at 72 °C. This was repeated for 40 cycles (*c-myb*) and 28 cycles (β-actin), with final extension period of 3 min. Primer sequences were as follows: *c-myb*, 5′-AAT TAA ATA CGG TCC CCT GAA 3′ (forward), 5′-TGC TCC TCC ATC TTT CCA CAG-3′ (reverse), 423 bp predicted product size; and β-actin, 5′-GGC TAC AGC TTC ACC ACC AC-3′ (forward), 5′-AGG GCA GTG ATC TCC TTC TG-3′ (reverse), 370 bp predicted product size. PCT products were resolved by agarose gel electrophoresis and visualized by GelStar®. Amplified DNA fragments were quantified by a gel documentation system (Alpha DigiDOC gel documentation system, Alpha Innotech).

5.7. Confocal fluorescent microscopy

A375 cells (9×10^3 cells) were grown just before confluence in a glass-bottomed dish. Following addition of 1.09 mg/ml Texas Red®-labeled RGD(1.3)-SPG/5′-FITC-labeled (dA_{50}) (1 μl) to the medium (100 μl), the cells were incubated for 6 h at 37 °C in a 5% CO_2 incubator. The cells were then washed twice with PBS (125 μl), and fixed with 5% HCHO (90 μl) at 4 °C for 20 min. The cells were treated with one drop of the antifade solution and examined by fluorescence microscopy. Images of the samples were collected by fluorescence microscopy on IX-70 (Olympus, Tokyo, Japan) attaching a confocal scan unit CSU-10 (Yokogawa, Tokyo, Japan) with ORCA-ER CCD Camera (Hamamatsu Photonics, Hamamatsu, Japan) using a 40× Uapo/340 objective with NA 0.9. 5′-FITC-labeled (dA_{50}) was obtained from Proligo Japan (Kyoto, Japan) and Texas Red® hydrazine and Fluorescence antifade kit (SlowFade®) were purchased from Molecular Probes (Eugene, OR). The preparation of the Texas Red®-labeled SPG is described elsewhere [29].

Acknowledgements

This work is financially supported by "Organization and Function", PRESTO, and SORST programs in Japan Science and Technology Corporation (JST).

References

[1] E. Uhlmann, A. Peyman, Chem. Rev. 90 (4) (1990) 543–584.
[2] C.A. Stein, Y.C. Cheng, Science 261 (1993) 1004–1012.
[3] T.V. Chirila, P.E. Rakoczy, K.L. Garrett, X. Lou, I.J. Constable, Biomaterials 23 (2) (2002) 321–342.
[4] C.A. Stein, A.M. Krieg, Antisense Res. Dev. 4 (1994) 67–69.
[5] C.A. Stein, A.M. Krieg, Applied Antisense Oligonucleotide Technology, Wiley-Liss, New York, NY, 1998.
[6] S. Mani, C.M. Rudin, K. Kunkel, J.T. Holmlund, R.S. Geary, H.L. Kindler, F.A. Dorr, M.J. Ratain, Clin. Cancer Res. 8 (4) (2002) 1042–1048.
[7] M.C. Cripps, A.T. Figueredo, A.M. Oza, M.J. Taylor, A.L. Fields, J.T. Holmlund, L.W. McIntosh, R.S. Geary, E.A. Eisenhauer, Clin. Cancer Res. 8 (7) (2002) 2188–2192.
[8] J.P. Leonetti, G. Degols, J.P. Clarenc, N. Mechti, B. Lebleu, Prog. Nucleic Acid Res. 44 (1993) 143–166.
[9] J.P. Clarenc, G. Degols, J.P. Leonetti, P. Milhand, B. Lebleu, Anti-Cancer Drug Des. 8 (1993) 81–94.
[10] R.L. Juliano, S. Akhtar, Antisense Res. Dev. 2 (1992) 165–176.
[11] D.C. Litzinger, J. Liposome Res. 7 (1997) 51–61.
[12] R. DeLong, K. Stephenson, T. Loftus, M. Fisher, S. Alahari, A. Nolting, R.L. Juliano, J. Pharm. Sci. 86 (1997) 762–764.
[13] O. Boussif, F. Lezoualch, M.A. Zanta, M.D. Mergny, D. Scherman, B. Demeneix, J.P. Behr, Proc. Natl. Acad. Sci. U. S. A. 92 (1995) 7297–7301.
[14] D. Putnam, C.A. Gentry, D.W. Pack, R. Langer, Proc. Natl. Acad. Sci. U. S. A. 98 (2001) 1200–1205.
[15] Y. Kakizawa, A. Harada, K. Kataoka, Biomacromolecules 2 (2001) 491–497.
[16] S. Vinogradov, E. Batrakova, S. Li, A. Kabanov, Bioconjug. Chem. 10 (5) (1999) 851–860.
[17] M.A. Maier, C.G. Yannopoulos, N. Mohamed, A. Roland, H. Fritz, V. Mohan, G. Just, M. Manoharan, Bioconjug. Chem. 14 (2003) 18–29.
[18] T. Azzam, H. Eliyahu, L. Shapira, M. Linial, Y. Barenholz, A.J. Domb, J. Med. Chem. 45 (9) (2002) 1817–1824.
[19] K. Sakurai, S. Shinkai, J. Am. Chem. Soc. 122 (18) (2000) 4520–4521.
[20] K. Sakurai, M. Mizu, S. Shinkai, Biomacromolecules 2 (3) (2001) 641–650.
[21] K. Tabata, W. Ito, T. Kojima, Carbohydr. Res. 89 (1981) 121–135.
[22] T. Norisuye, T. Yanaki, H. Fujita, J. Polym. Sci., Polym. Phys. Ed. 18 (1980) 547–558.
[23] T. Yanaki, T. Norisuye, H. Fujita, Macromolecules 13 (1980) 1462–1466.
[24] T. Sato, K. Sakurai, T. Norisuye, H. Fujita, Polym. J. 15 (1983) 87–96.
[25] T.M. McIntire, D.A. Brant, J. Am. Chem. Soc. 120 (1998) 6909–6914.
[26] T. Kimura, K. Koumoto, K. Sakurai, S. Shinkai, Chem. Lett. (2000) 1242–1243.
[27] K. Koumoto, T. Kimura, H. Kobayashi, K. Sakurai, S. Shinkai, Chem. Lett. (2001) 908–909.
[28] R. Kobayashi, K. Sakurai, T. Kimura, K. Koumoto, M. Mizu, S. Shinkai. Abstracts of the 2001 Spring Meeting for Japan Polymer Society. (The English manuscript is in preparation).
[29] M. Mizu, K. Koumoto, T. Kimura, T. Nagasaki, K. Sakurai, S. Shinkai, J. Control Release (submitted for publication).
[30] Y. Shimizu, J.T. Chen, K. Hasume, K. Masubuchi, Biotherapy 4 (1990) 1390–1399.
[31] M. Colin, R.P. Harbottle, A. Knight, M. Komprobst, R.G. Cooper,

A.D. Miller, G. Turgnan, J. Capeau, C. Coutelle, M.C. Brahimi-Horn, Gene Ther. 5 (1998) 1488–1498.
[32] S. Futaki, I. Nakase, T. Suzuki, Z. Youjun, Y. Sugiura, Biochemistry 41 (2002) 7925–7930.
[33] T. Suzuki, S. Futaki, M. Niwa, S. Tanaka, K. Ueda, J. Biol. Chem. 277 (2002) 2437–2443.
[34] K. Koumoto, T. Kimura, M. Mizu, K. Sakurai, S. Shinkai, Chem. Commun. (2001) 1962–1963.
[35] K. Sakurai, K. Koumoto, M. Miz, S. Shinkai, ACS National Meeting Preprints, Biomaterials (Submitted for publication).
[36] R.P. Isberg, G. Tran Van Nhieu, Trends Cell Biol. 5 (1995) 120–124.
[37] D. Logan, et al., Nature 362 (1993) 566–568.
[38] K. Sakurai, R. Iguchi, M. Mizu, K. Koumoto, S. Shinkai, Bioorganic Chem. (in press).
[39] R.I. Mahato, Y. Takakura, M. Hashida, J. Drug Target. 4 (1997) 337–357.
[40] M. Numata, T. Matumoto, M. Umeda, K. Koumoto, K. Sakurai, S. Shinkai, Bioorganic Chem. 31 (2003) 163–171.
[41] B. Majello, L.C. Kenyon, R. Dalla-Favera, Proc. Natl. Acad. Sci. U. S. A. 83 (1986) 9636–9640.
[42] A.J. Linnenbach, K. Huebner, E.P. Reddy, M. Herlyn, A.H. Parmiter, P.C. Nowell, H. Koprowski, Proc. Natl. Acad. Sci. U. S. A. 85 (1988) 74–78.
[43] A.M. Gewirtz, B. Calabretta, Science 242 (1988) 1303–1306.
[44] N. Hijiya, J. Zhang, M.Z. Ratajczak, J.A. Kant, K. DeRiel, M. Herlyn, G. Zon, A.M. Gewirtz, Proc. Natl. Acad. Sci. U. S. A. 91 (1994) 4499–4503.
[45] G. Sergei, S. Tomasz, C. Carla, N.S. Malorzata, Y.C. Choi, L. David, C. Jer-Kang, K. Maria, C. Bruno, Proc. Natl. Acad. Sci. U. S. A. 24 (8) (1996) 1508–1514.
[46] F. Pastorino, D. Stuart, M. Ponzoni, T.M. Allen, J. Control. Release 74 (1–3) (2001) 69–75.
[47] M. Mizu, T. Kimura, K. Koumoto, K. Sakurai, S. Shinkai, Chem. Commun. (2001) 429–430.
[48] Invitorogen No. 18057N.
[49] T. Hiraoka, I. Hamachi, Bioorg. Med. Chem. Lett. 13 (2003) 13–15.
[50] I.J. Moon, Y. Lee, C.S. Kwak, J.H. Lee, K. Chol, A.D. Schreiber, J.G. Park, Biochem. J. 346 (2000) 295.

Available online at www.sciencedirect.com
SCIENCE DIRECT®
Carbohydrate Research 339 (2004) 251–258
Carbohydrate RESEARCH

Rod-like architecture and helicity of the poly(C)/schizophyllan complex observed by AFM and SEM ☆

Ah-Hyun Bae,[a] Seung-Woo Lee,[b] Masato Ikeda,[a] Masahito Sano,[c] Seiji Shinkai[a] and Kazuo Sakurai[b,*]

[a]*Department of Chemistry and Biochemistry, Graduate School of Engineering, Kyushu University, Fukuoka 812-8581, Japan*
[b]*Department of Chemical Processes and Environments, Faculty of Environmental Engineering, The University of Kitakyushu, Sakurai Laboratory, 1-1 Hibikino, Wakamatsu-ku, Kitakyushu-shi, Fukuoka-ken 808-0135, Japan*
[c]*Department of Polymer Science and Engineering, Yamahata University, Yonezawa 992-8510, Japan*

Received 27 May 2003; accepted 23 September 2003

Abstract—Microscopic studies of the complex between poly(C) and schizophyllan (SPG), employing both AFM and SEM, revealed that the complex takes the same rod-like architecture on the mica surface as those of the renatured SPG and the original triple helix of SPG, indicating that the complex also has a helical structure. The SEM observations showed the helical pattern on the rod surface, only when the sample was metal shadowed. The pitch evaluated from the image is comparable with that obtained from crystallographic data. The ability to visualize the helical structure can be explained from the hypothesis that the platinum grains may assemble on the sample using the molecular surface of the SPG (or complex) as the template.

Keywords: AFM; SEM; Schizophyllan; Poly(C); Complex; Rod-like architecture; Helicity

1. Introduction

Schizophyllan is a cell-wall polysaccharide produced by the fungus *Schizophyllum commune*. The main chain consists of β-(1→3)-D-glucan with one β-(1→6)-D-glucosyl side chain linked to the main chain at every three glucose residues (see Fig. 1a).[2] Norisuye and coworkers[3,4] showed that schizophyllan adopts a triple helical conformation (see Fig. 1b) in water and a random coil in dimethyl sulfoxide (Me_2SO). When water is added to the Me_2SO solution (renaturation), the single chain of schizophyllan (s-SPG) collapses owing to formation of hydrogen bonds.[5] McIntire and Brant[6] and Young and Dong[7] independently showed that the triple helical structure can be retrieved when the renaturation process is carried out in considerably dilute solutions (ca. 4–30 μg/mL). Recently, Sakurai and Shinkai[1,8–10] found that s-SPG forms a macromolecular complex with poly(C) when the polynucleotide is present in the renaturation process. They found that the complexation proceeds in a highly stoichiometric manner that is to say, two schizophyllan repeating units and three poly(C) units are bound in the complex.[9] This stoichiometric number can be interpreted in terms of two SPG chains and one poly(C) chain forming a new triple helix structure.[9,10]

According to X-ray crystallographic studies,[11–13] the triple helical schizophyllan (t-SPG) and the single chain of poly(C) form a right handed 6_1 triple helix with a 1.8 nm pitch and a right handed 6_1 helix with a 1.86 nm pitch, respectively. Since both helix parameters are surprisingly similar, we can assume that the helix formation from poly(C) and s-SPG chains may not induce either a large conformational change or an unfavorable entropy gain. If an enthalpy driving force (such as charge transfer or hydrogen bonding) is present between

☆ Polysaccharide–polynucleotide complexes,[1] Part 18.

* Corresponding author. Tel.: +81-93-695-3294; fax: +81-93-695-3298; e-mail addresses: sakurai@env.kitakyushu-u.ac.jp, sakurai@env.kitakyu-u.ac.jp

0008-6215/$ - see front matter © 2003 Elsevier Ltd. All rights reserved.
doi:10.1016/j.carres.2003.09.032

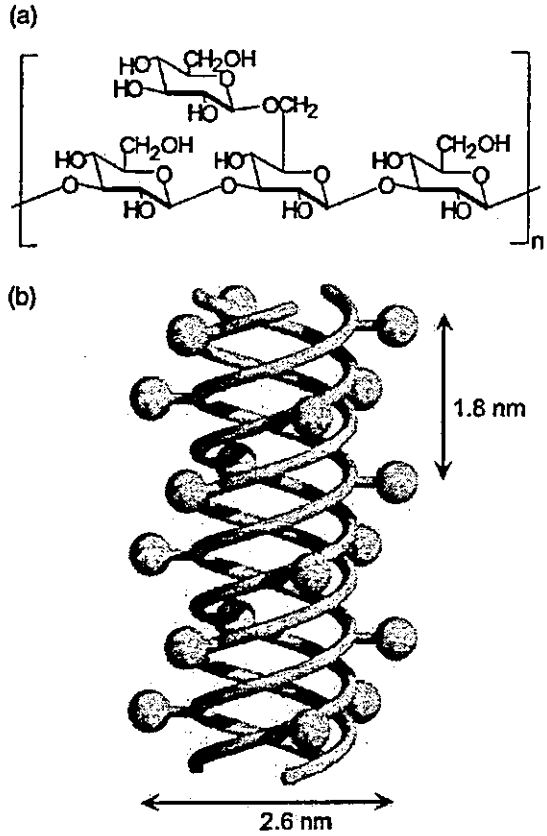

Figure 1. Repeating unit of schizophyllan (a) and a representative model of the triple helix (b); the balls represent the side chains.

poly(C) and s-SPG, two different chains can form a helical complex. In fact, our previous work[9] showed that the hydrogen-bonding interaction plays an important role in the complexation. Using the Discover 3 program, we took out one glucan chain from t-SPG and tried to fit one poly(C) chain into the groove occupied by the absent glucan.[10] We found that replacing one glucan chain by the poly(C) chain can be achieved easily without inducing significant steric hindrance. After replacing the glucan chain with poly(C), the most stable conformation for poly(C) in the groove was determined by molecular mechanics using the Amber force field, and the resultant structure is shown in Figure 2.[10] The glucan chains are presented by the CPK model and the poly(C) chain by a ball-and-stick model. As shown in the figure, the ribose takes 3′-endo conformation and the fourth amino group in the cytosine comes close enough to the second oxygen in s-SPG to form a hydrogen bond. All the above results are consistent with the speculation that the poly(C)/s-SPG complex forms a triple helix and that the helix parameter is similar to that of t-SPG. However, all of these results are still circumstantial evidence. The purpose of this paper is to present more direct visual evidence on the nature of the molecular complex.

Microscopic observation of biomolecules is a challenging issue,[14,15] and much work has been dedicated toward observation of the double helix of DNA.[15–17] Only a few papers have so far suggested that true helicity of the DNA structure can be seen with atomic force microscopy (AFM).[15,16] The difficulty is caused by the fact that the radius of the tips are generally larger than the pitch of the helix, and that the structure of the molecules is generally fairly flexible, and probably distorted by the imaging process. There are a considerable number of rod-like polysaccharides that have been imaged by AFM, including xanthan,[18] acetan,[19] gellan,[20] amylose,[21] and carrageenans.[21] However, due to the imperfect tip reading and the distorted image, there are only a few studies on acetan that show helical repeats consistent with that of X-ray diffraction data.[19] McIntire and Brant[6] and Stokke et al.[22] independently observed three β-(1→3)-D-glucans (scleroglucan, schizophyllan, and lentinan) with AFM and found that the natural glucans exhibit a rod-like architecture, which is expected from the studies on the dilute solution properties of those polymers. They also showed that the renatured materials may appear as macrocycles, depending on the

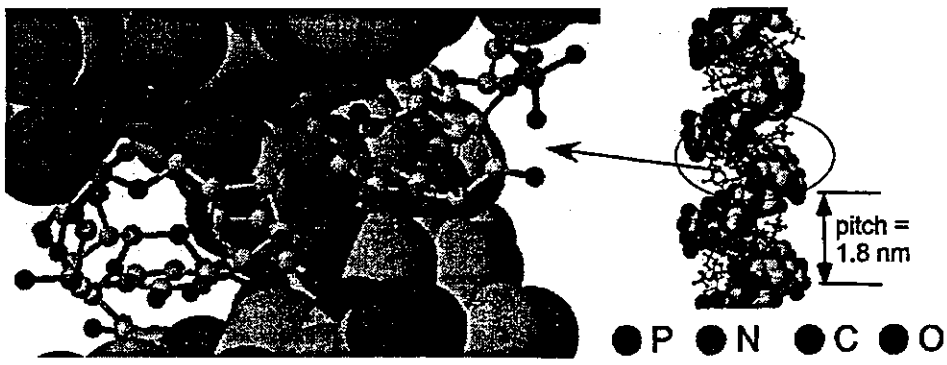

Figure 2. The most stable structure for the poly(C)/s-SPG complex obtained by molecular mechanics calculations. The glucan chains are presented by the CPK model and the poly(C) chain by a ball-and-stick model.

renaturing conditions.[6] However, the resolution was not good enough to observe the helicity of these polysaccharides. Kunitake and Ohira[23] used AFM to observe the conformation of schizophyllan. They reported some helical pattern on the molecule; however, the observed helicity was not consistent with the crystallographic data.

If the speculation that the complex forms a novel triple helix is valid, then we should be able to see a rod-like architecture for the complex. In this work, using both AFM and scanning electron microscopy (SEM), we have imaged the molecular architecture of the poly(C)/schizophyllan complex and compared it with that seen for renatured schizophyllan.

2. Results and discussion

2.1. AFM observation and rod-like architecture of the complex

Figure 3 compares the AFM images obtained when the s-SPG/poly(C) molar ratio is varied from 0 to 1.0. When the ratio is 1.0:0 (only renatured s-SPG, Panel 1), the image shows a mixture of rods and rings. Although the results are not presented, the image for t-SPG showed only rods with a similar length to that of the rods in Panel 1. The height of each rod or ring is about 2–3 nm, being consistent with that for the schizophyllan triple helix. The data shown in Panel 1 is consistent with that in reported studies for the renatured s-SPG samples.[6,18,22] All the experimental facts indicate that the rod represents the molecule, namely, a triple helix has been made from s-SPG in the renaturation process. We measured the contour length of the rods (L) in this panel as well as other AFM images taken under the same conditions, and plotted the results as the distribution of L in Figure 4B. For comparison, the distribution of L for t-SPG is presented in Figure 4A.

Using the gamma distribution (see the Experimental section), we evaluated the most suitable parameters to provide the matched distribution for the data, and the result is presented by the solid line. For both t-SPG and s-SPG, the data points are well fitted by a standard gamma distribution with $\alpha = 4.4$ (when $x = L/40$). Table 1 summarizes the number average L and the number-average molecular weight (M_n) and the weight-average molecular weight (M_w). All the statistical data for the renatured s-SPG agree with those of the original triple helix, indicating that the rod-like images in Panel 1 represent individual molecules, and the molecules have an equivalent molecular weight and distribution to those of the original triple helix. This fact evidences that the renaturation occurred via three individual s-SPG chains. Both M_n and M_w listed in the table are approximately 20% larger than those determined from gel-permeation chromatography (see the Experimental section). This discrepancy may be ascribed to an experimental error due to different technique, or suggests that we could not omit the aggregates completely when we measured L. There is a minor second maximum (or deviation from the gamma distribution) in the range of 300–400 nm. The origin of this maximum may be the molecular aggregates. There are some rings observed in Panel 1 as minor species. As has previously been pointed out,[6] these images are probably made from one or two s-SPG chains due to ring closure. When we measured the length of the molecules, we omitted these rings.

Panel 5 in Figure 3 shows the image obtained for poly(C). This consists of only circular dots, which seems typical for flexible chains.[24] Therefore, we can consider that the circular dots represent poly(C) molecules that are not involved in complexation with s-SPG. When we observed three mixtures of poly(C) and s-SPG (Panels 2–4), the rod population decreased and the dot population increased with increasing the poly(C) composition. However, even for the stoichiometric mixture (Panel 3), dots are observed. Hence the question needs to be asked whether the rod in the mixture represents the poly(C)/s-SPG complex or simply renatured s-SPG. In Panel 2 [the ratio = 4.5:1.0, the poly(C) composition is less than stoichiometric], there are no dots, suggesting that most poly(C) molecules are incorporated into the rods due to the complexation. Furthermore, rings in Panels 3 and 4 were less abundant than in the renatured s-SPG (Panel 1). The mixing of poly(C) and s-SPG was carried out in a nonsalt aqueous solution. Therefore, if the complex is formed, the electrostatic repulsion between the phosphate anions in poly(C) might hinder ring closure reactions. Although these features are consistent with complex formation, this evidence is not sufficient to prove that the rods represent complexes.

Measurements of L were made for the rods in Panel 4, as well as for the other AFM images taken under the same conditions. Figure 4C shows the distribution. By comparing this histogram with the others (t-SPG and s-SPG), it can be seen that the mixture has a different length distribution to those of the renatured s-SPG and t-SPG, indicating that the mixture has longer rods than the renatured s-SPG. This difference supports the suggestion that the presence of poly(C) influences the rod length through complexation. It is interesting that the mixture has a second maximum about the 300–350 nm length. Since poly(C) has 570 bases, the extended poly(C) chain is about 200 nm long, and that of s-SPG is about 180 nm long. Therefore, the second maximum around 300–350 nm can appear only when more than two s-SPG chains are involved in the complexation, as illustrated in the figure.

In order to fit the data for the mixture, we have to assume multiple distributions. In this work, we assumed two gamma functions; the first function is the same as that for the s-SPG, and the second one is a gamma

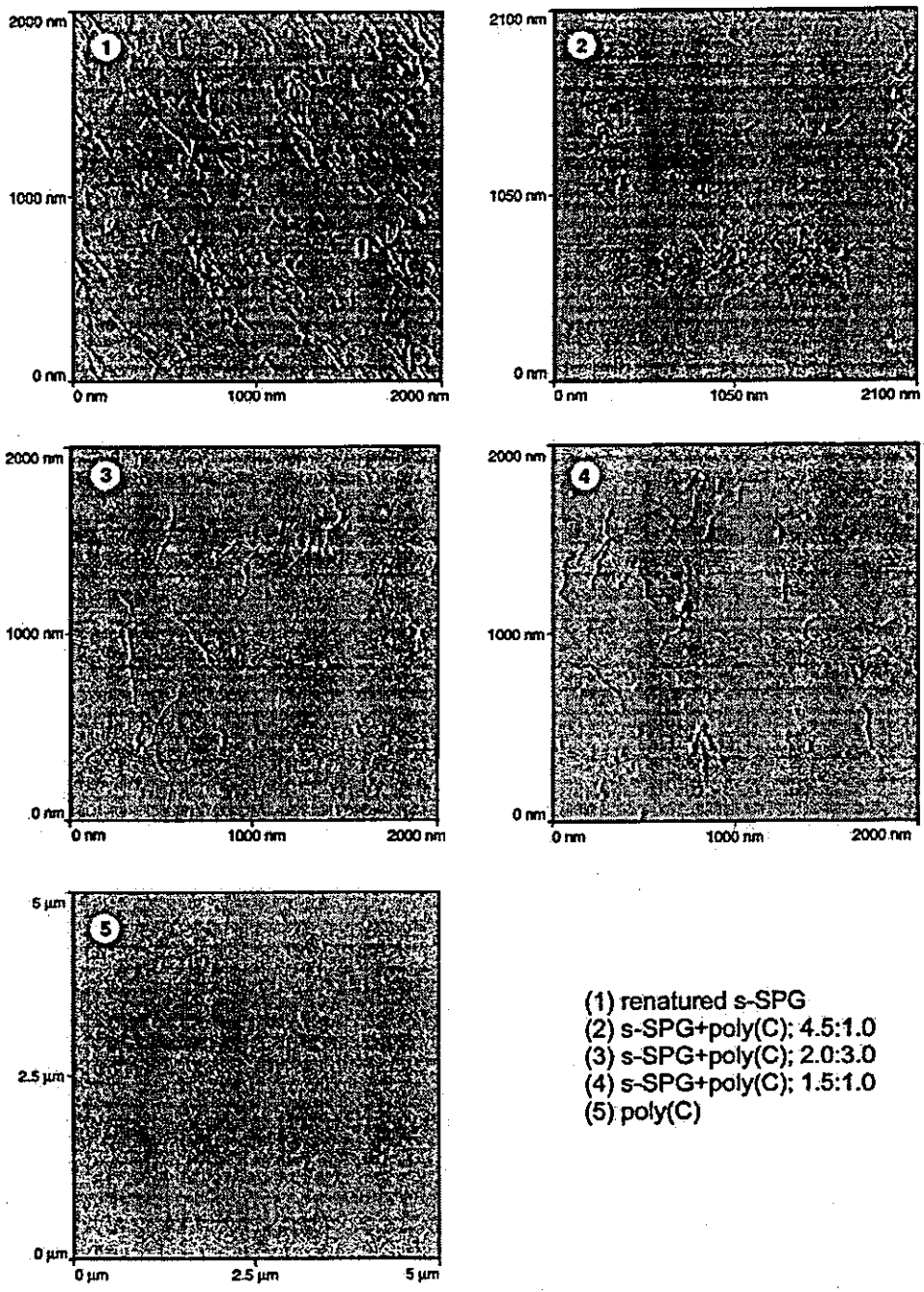

Figure 3. Comparison of the AFM images obtained when the s-SPG/poly(C) ratios are 1.0:0 (1), 4.5:1.0 (2), 2.0:3.0 (3), 1.5:1.0 (4), and 0:1.0 (5).

function with $\alpha = 4.4$ and $\beta = 1.0$. By iterating, we reached the conclusion that the measured distribution consists of 80% of the first one and 20% of the second. As a matter of fact, the second function can be any function such as the Poisson distribution. The important conclusion is that the mixture has a different length distribution from those of the renatured s-SPG and t-SPG, and 20% of the rods are almost twice as lon g as the original SPG. Furthermore, the complex exhibits a very long rods with $L > 500$ nm. This may be due to three helixes being connected with poly(C), as depicted in the figure.

2.2. SEM observation and the metal-grain array reflecting the molecular helicity

Figure 5 shows a typical SEM image for t-SPG. The thickness of the platinum coating (estimated from the coating time and current) is 16 nm, and the average size (diameter) of the rod-like image (d_t) is 20 ± 2 nm.

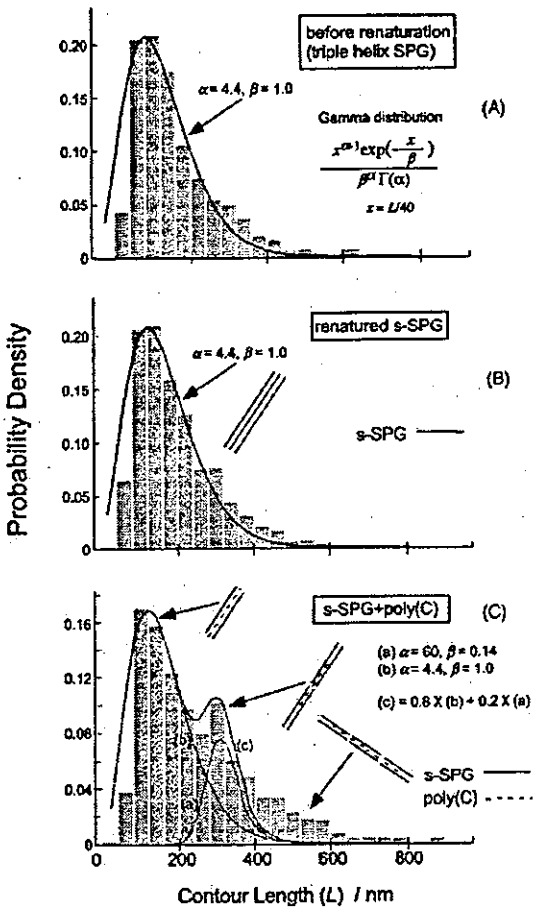

Figure 4. Comparison of the rod length distribution among the original triple helix (A), the renatured s-SPG (B) and the poly(C)/s-SPG mixture (C). The solid lines in (A) and (B) represent the standard gamma function with $\alpha = 4.4$ and $\beta = 1$. The solid lines (a) and (b) in Panel C represent the gamma functions with $\alpha = 60$ and $\beta = 0.14$, and $\alpha = 4.4$ and $\beta = 1$, respectively. The solid line (c) is the convoluted distribution curve made from the lines (a) and (b). The inserted illustrations in the panel schematically show a possible molecular aggregate consistent with the distribution. The complex contains longer rods as the minor species, which is considered to be made from more than two s-SPG chains, whereas, the renatured schizophyllan is mainly made from three s-SPG chains. The different distribution between (B) and (C) evidences the complex formation.

Table 1. Molecular weight and its distribution estimated from the AFM images

Sample	Number average L/nm	$M_n/10^4$	$M_w/10^4$	M_w/M_n
t-SPG (from AFM)	215	46.7	55.8	1.2
s-SPG(from AFM)	220	47.7	59.3	1.2
s-SPG/poly(C) (from AFM)	262	56.9	72.7	1.3
t-SPG (from GPC)	—	36.0	45.0	1.3

Therefore, the actual diameter of the t-SPG sample is ~2–6 nm, which is larger than the crystallographic data (2.6 nm).[11,12] It is interesting that we observe the image

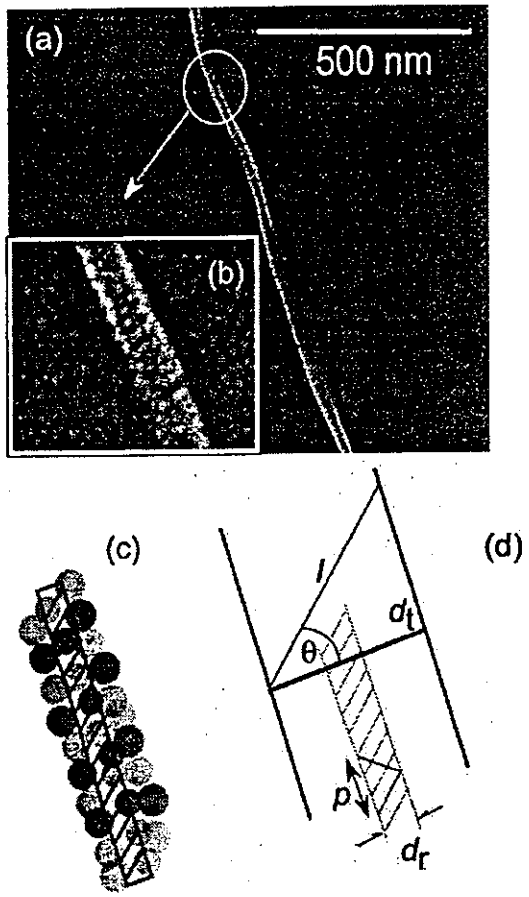

Figure 5. A SEM image of the triple helix of schizophyllan (a) and a magnified image (b). Panel c is a model that shows the platinum grains are arrayed using the molecular surface as the template, and Panel d presents the definitions of the lengths and angles. The incremental angle θ is determined by $\theta = \cos^{-1}(I/d_t)$, where I and d_t are the length of the grain array and the diameter of the image, respectively. The definitions of p and d_r are described in the text.

that, the platinum grains attached onto the sample, array regularly with a fixed value of the inclination angle relative to the rod axis. Through examination of several samples, we confirmed that the helical pattern is always right handed, being consistent with the expected helicity of t-SPG. The essential process acquired to obtain such a pattern is metal shadowing (see the Experimental section). The averaged inclination angle (θ) was evaluated to be 20–25° from Figure 5, as well as from other images taken under the same conditions, using the equation of $\theta = \cos^{-1}(I/d_t)$, where I is the length of the grain array (see Panel d in Fig. 5). Thus the value of θ so obtained can be related to the helix pitch (p) and the diameter of the real molecule (d_r) with the following equation:

$$p = 2d_r \tan(\theta). \quad (1)$$

Using Eq. 1, p can be evaluated to be between 2.0 and 2.4 nm, where d_r is the diameter of the real molecule; therefore, we use the crystallographic data: $d_r = 2.6$ nm.

This value of p is relatively larger than the crystallographic pitch (1.8 ± 0.1 nm).[12] By taking account of ambiguity involved in the present evaluation of p, the value obtained from AFM can be considered to be in the same order as that of the crystallographic data. All the above discussions on the SEM observations conclude that the array of platinum grains reflects the helicity of the triple helix of schizophyllan.

The finest resolution of the SEM observation is usually only a few nm, which is determined by the size of the metal grain. In fact, the platinum grain size in our picture ranges ~4–5 nm. Therefore, one might consider that it is strange to be able to achieve 2-nm resolution in our SEM observation, that is, to be able to observe the 1.8 nm pitch of t-SPG. We evaluated the pitch not directly but through the inclination of the metal-grain array using Eq. 1. It is true that the helical image in the SEM picture is incontrovertible (see Panel b in Fig. 5) and that we frequently observe such a pattern. We presume that when we coat the sample with platinum grains by shadowing, they are caught by the side chains of the schizophyllan, which should stick out from the molecules. In other words, the platinum grains array on the surface of t-SPG using the molecular helicity as a template (see Panel c in Fig. 5).

Figure 6 shows an image from the renatured s-SPG. This image exhibits a rod-like architecture, and the surface also shows a helical pattern. Although the helical resolution is poorer than that of t-SPG, we can confirm that the value of p is in the range of 2–3 nm. Although not shown, sometimes we observed rings in the SEM images, which is consistent with the AFM results.

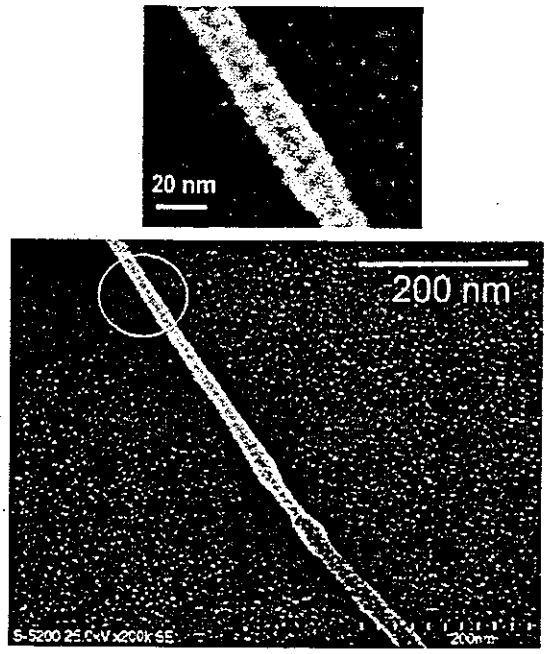

Figure 6. SEM images of the renatured schizophyllan showing the rod architecture and its magnification.

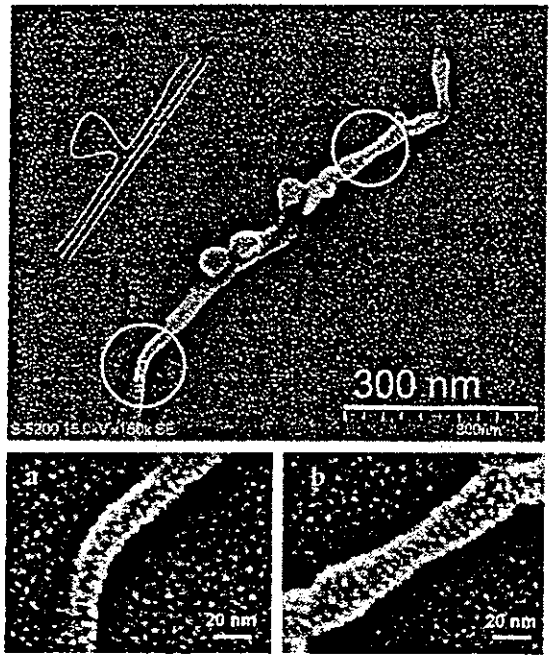

Figure 7. SEM images of the stoichiometric poly(C)/s-SPG complex. The upper image shows small bumps observed for the complex and a model for this architecture, and the lower images show magnification of the circled part of the image.

The stoichiometric complex of poly(C) and s-SPG shows somehow different features from that of the renatured s-SPG. Rings were less abundant than in the renatured sample, similar to the AFM observation. Instead of linear strands, small bumps were frequently observed on the rod-like images, as shown in Figure 7. The bumps on the rods may correspond to a defect of the complex, as illustrated in the insert of the figure. When the image of the strand is magnified, the same helical pattern is observed. The calculated pitch approximately agrees with that for t-SPG, although there is a relatively large experimental error. This helix pattern and agreement of the pitch length suggest that the poly(C)/s-SPG complex forms a triple helix with the same parameters as that of the original t-SPG.

The resolution of the images in Figures 6 and 7 is not as good as that in Figure 5. This reason could be that the side chains in the renatured s-SPG or complex line up less perfectly than those in the original triple helix depicted in Figure 1b.

3. Conclusions

The AFM and SEM observations reveal that the complex between poly(C) and schizophyllan forms the same rod-like architecture as for the renatured s-SPG and t-SPG,

indicating that a rod-like aggregate is formed upon complexation. The SEM observations show the helical pattern on the rod surface only when the sample was shadowed. The pitch evaluated from the image is comparable with that of the crystallographic data for t-SPG. The present microscopic studies indicate that the complex is a helical structure similar to that of t-SPG.

4. Experimental

4.1. Materials and complexation

Taito Co. in Japan kindly supplied the triple helical schizophyllan sample (t-SPG). The weight-average molecular weight (M_w) and the molecular weight distribution (defined by M_w/M_n where M_n is the number-average molecular weight) for the t-SPG sample, determined with gel-permeation chromatography (GPC) by use of a HLC-8020 (TOSOH), were 4.6×10^5 and 1.2–1.3, respectively. M_w and the number of repeating units for the single chain of SPG (s-SPG), evaluated from the intrinsic viscosity measurement in Me_2SO,[3,4] were 1.5×10^5 and 231 (in terms of the number of main chain glucose, 690 units), respectively. Poly(C) with the number of base = 570 was purchased from Amersham Pharmacia. The complex was prepared by mixing poly(C)/water with s-SPG/Me_2SO solutions, and then the solution was dialyzed for 48 h to remove Me_2SO. The complex solution was diluted to less than 2.6×10^{-3}–1×10^{-4} wt% and ultrasonicated for 5 min.

4.2. Electron microscopy observations

Dilute solutions of the original (natural) schizophyllan (t-SPG), renatured s-SPG, and poly(C)/s-SPG complex were cast onto freshly cleared mica, and the cast films were allowed to stand in clean air at room temperature in order to evaporate the solvent. The films were imaged by AFM (TopoMetrix) operating in a noncontact mode at room temperature, using a Si_3N_4 pyramidal tip (Cantilever Ultrasharp™ Silicium Cantilever). Field emission scanning electron microscopy (FE-SEM) was conducted with a Hitachi S-5200 instrument at an acceleration voltage of 15–25 kV. For the SEM observation, some of the metal-coated mica samples were initially frozen with liquid nitrogen for 5 min and then dried in vacuum. This freeze-drying procedure did not create any significant artificial effects. The mica samples were attached on the SEM specimen, and the specimen was positioned horizontally to the heated tungsten filament in the vacuum chamber. The specimen was coated with platinum for 5 s from both sides and subsequently coated vertically for 70 s, using a Hitachi E-1030 ion sputter (15 mA, 10 Pa). This shadowing technique was necessary in order to observe the molecules; otherwise, the molecules seemed to be buried in the platinum grains. The thickness of the metal coat was evaluated from the coating time and the current.

4.3. Statistical analysis of the AFM images

We measured the contour length (L) of the rod-like images in the AFM pictures using a flexible ruler. In the measurements we omitted dots, circles, and aggregates by judging width and shape. Since the distribution of L versus population obtained from AFM images had a similar shape with that of the gamma distribution, we fitted the histogram using the following equation:

$$f(x) = \frac{x^{\alpha-1}\exp\left(-\frac{x}{\beta}\right)}{\beta^{\alpha}\Gamma(\alpha)}, \quad (2)$$

where $f(x)$, α, β, and $\Gamma(\alpha)$ are the probability distribution function, the shape parameter, scale parameter, and the gamma function, respectively. The case where $\beta = 1$ is called the standard gamma distribution. For convenience, we defined $x = L/40$ and obtained the most matched curve for the data by regression analysis. To convert L to the molecular weight, the molar mass per unit contour length (M_L) of the schizophyllan triple helix was assumed to be 2170 nm^{-1} (according to Kashiwagi et al.[25]), and the equation of $L = M/M_L$ was used.

Acknowledgements

This work has been financially supported by SORST and PRESTO program of the Japan Science and Technology Corporation. The present SEM work was carried out at Instrumentation Center at the University of Kitakyushu.

References

1. Mizu, M.; Koumoto, K.; Kimura, T.; Sakurai, K.; Shinkai, S. *Polymer J.* **2003**, *35*, 714–720.
2. Takaba, K.; Ito, W.; Kojima, T.; Kawabata, S.; Misaki, A. *Carbohydr. Res.* **1981**, *89*, 121–135.
3. Norisuye, T.; Yanaki, T.; Fujita, H. *J. Polym. Sci. Polym. Phys. Ed.* **1980**, *18*, 547–558.
4. Yanaki, T.; Norisuye, T.; Fujita, H. *Macromolecules* **1980**, *13*, 1462–1466.
5. Sato, T.; Sakurai, K.; Norisuye, T.; Fujita, H. *Polym. J.* **1983**, *15*, 87–96.
6. McIntire, T. M.; Brant, D. A. *J. Am. Chem. Soc.* **1998**, *120*, 6909–6919.
7. Young, S. H.; Dong, W. J. *J. Biol. Chem.* **2000**, *275*, 11874–11879.
8. Sakurai, K.; Shinkai, S. *J. Am. Chem. Soc.* **2000**, *122*, 4520–4521.
9. Sakurai, K.; Mizu, M.; Shinkai, S. *Biomacromolecules* **2001**, *2*, 641–650.

10. Sakurai, K.; Shinkai, S. *J. Inclusion Phenom.* **2001**, *41*, 173–178.
11. Deslandes, Y.; Marchessault, R. H.; Sarko, A. *Macromolecules* **1980**, *13*, 1466–1471.
12. Bluhm, T. L.; Deslandes, Y.; Marchessault, R. H.; Pérez, S.; Rinaudo, M. *Carbohydr. Res.* **1982**, *100*, 117–130.
13. Saenger, W. *Principles of Nucleic Acid Structure*; Springer: New York, 1984; Chapter 13.
14. Merkel, R. *Phys. Rep.* **2001**, *346*, 343–385.
15. Hansma, H. G. *Biophys. J.* **1995**, *68*, 1672–1677.
16. Hansma, H. G.; Laney, D. E.; Bezanilla, M.; Sinsheimer, R. L.; Hansma, P. K. *Biophys. J.* **1995**, *68*, 1672–1677.
17. Mou, J.; Czajikowsky, D. M.; Yiyi, Z.; Zhifeng, S. *FEBS Lett.* **1995**, *371*, 279–282.
18. Camesano, T. A.; Wilkinson, K. J. *Biomacromolecules* **2001**, *2*, 1184–1191.
19. Kirby, A. R.; Gunning, A. P.; Ridout, M. J. *Biophys. J.* **1995**, *68*, 358–362.
20. Morris, V. J.; Mackie, A. R.; Wilde, P. J.; Kirby, A. R.; Mills, E. C. N.; Gunning, P. A. *Leben.-Wissen. Technol.* **2001**, *34*, 3–10.
21. McIntire, T. M.; Brant, D. A. *Int. J. Biol. Macromol.* **1999**, *26*, 303–310.
22. Stokke, B. T.; Elgsaeter, A.; Kitamura, S. *Polym. Gel Networks* **1994**, *2*, 173–190.
23. Kunitake, M.; Ohira, A. *Kobunshi* **2002**, *51*, 240–244; *Chem. Abstr.* **2002**, *137*, 310456.
24. Tasker, S.; Matthijs, G.; Davies, M. C.; Roberts, C. J.; Schacht, E. H.; Tendler, S. J. B. *Langmuir* **1996**, *12*, 6436–6442.
25. Kashiwagi, Y.; Norisuye, T.; Fujita, H. *Macromolecules* **1981**, *14*, 1220–1225.

Available online at www.sciencedirect.com
SCIENCE DIRECT®
Carbohydrate Research 339 (2004) 161–167
Carbohydrate RESEARCH

Note

Low M_w sulfated curdlan with improved water solubility forms macromolecular complexes with polycytidylic acid ☆

Kazuya Koumoto,[a] Mariko Umeda,[b] Munenori Numata,[b] Takahiro Matsumoto,[b] Kazuo Sakurai,[a] Toyoki Kunitake[a] and Seiji Shinkai[b,*]

[a]*Department of Chemical Processes and Environments, Faculty of Environmental Engineering, The University of Kitakyushu, 1-1 Hibikino, Wakamatsu-ku, Kitakyushu, Fukuoka 808-0135, Japan*
[b]*Department of Chemistry and Biochemistry, Graduate School of Engineering, Kyushu University, Fukuoka 812-8581, Japan*

Received 22 April 2003; revised 11 September 2003; accepted 12 September 2003

Abstract—The water solubility of curdlan was enhanced by partial sulfation at O-6. Circular dichroism measurements suggest that the sulfated curdlan with the degree of substitution (DS) from 0 to 8.7 mol% forms macromolecular complexes with polycytidylic acid (poly(C)). Although the thermal stability of the complexes decreased with increase in DS, this could be overlapped by addition of NaCl in the concentration above that of serum. The results clearly indicate that the drawback arising from the electrostatic repulsion between the anionic charges can be partially compensated by the presence of salt. Furthermore, the polynucleotide chain complexed with the sulfated curdlan was protected from the enzymatic hydrolysis, corroborating the assumption that the sulfated curdlan has an ability to bind poly(C).

Keywords: Curdlan; β-(1→3)-Glucan; Sulfation; Macromolecular complex; Polycytidylic acid

1. Introduction

We recently reported that schizophyllan (SPG, Fig. 1a), a β-(1→6)-branched β-(1→3)-glucan, can specifically form macromolecular complexes with certain polynucleotides.[2–5] As far as we know, this is the first example of a specific polysaccharide–polynucleotide interaction. This complex has several novel properties inherent to the macromolecular complex: they are; (i) the complex is dissociated in a cooperative manner upon heating similarly to DNA duplexes;[4] (ii) this complexation ability is induced only by the β-(1→3)-glucan skeleton;[6,7] (iii) the polynucleotide chain incorporated into the complex resists the enzymatic hydrolysis[8,9] and; (iv) the polynucleotide chain bound to the complex can be immediately replaced when it meets the complementary nucleotide chain.[10]

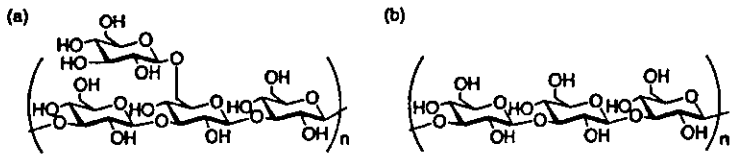

Figure 1. Comparative chemical structure of (a) schizophyllan and (b) curdlan.

☆ Polysaccharide–polynucleotide complexes,[1] Part 14.

* Corresponding author. Tel.: +81-92-642-3583; fax: +81-92-632-4357; e-mail: seijitcm@mbox.nc.kyushu-u.ac.jp

0008-6215/$ - see front matter © 2003 Elsevier Ltd. All rights reserved.
doi:10.1016/j.carres.2003.09.022

Among β-(1→3)-glucans, curdlan (Fig. 1b) is an inexpensive polysaccharide, which could find application in this area. We recently found that a low-molecular-mass curdlan prepared by acid hydrolysis is partially water soluble and forms complexes with certain RNAs and DNAs, although the commercially available curdlan ($M_w > 1{,}000{,}000$) is virtually insoluble in water and cannot form any complex with polynucleotides.[6,7] Taking its low cost into consideration, an appropriate modification of curdlan should improve its capability as polynucleotide binder.

From a viewpoint of application to gene technology, improvement of the water solubility is among the most crucial problems to be solved. In this report, we partially introduced sulfate groups in curdlan and evaluated its ability as polynucleotide binder.

2. Results and discussion

2.1. Synthesis of a sulfated curdlan

According to our recent results,[11] the complexation ability of curdlan appears in a limited M_w range window; the affinity for polycytidylic acid (poly(C)) was observed only in the M_w range from 1700 to 87,000 at $V_w = 0.75$, where V_w is the water volume fraction in the water–dimethylsulfoxide mixture. Taking this molecular mass effect and the purification easiness into account, it was desirable that curdlan with the molecular mass mentioned above could be prepared by acid hydrolysis.[7] In this study, the low-molecular-mass curdlan with $M_w = 24{,}800$ was used.

The synthesis of the sulfated curdlan was carried out in 0.25 M LiCl/Me_2SO solution using the pyridine–sulfur trioxide complex as the sulfation reagent (Scheme 1).[12] The degree of substitution (DS) was estimated by inductively coupled plasma (ICP) analysis using the sulfur oil standard solution (Aldrich) as a standard.† Thus, we could synthesize five sulfated curdlan samples with DS from 1.7 to 76 mol% based on glucose (Table 1). It should be emphasized that, as shown in Table 1, the DS values for our samples are very low compared with those obtained by Uryu and coworkers where DS values were ranging over 100 mol% in order to induce a biological response.[13,14]

It is already known that the thermal stability of the curdlan/polynucleotide complexes is affected by the M_w of curdlan and the strongest affinity appears in the M_w range from 8100 to 22,000.[11] Therefore, we compared the M_w values of the sulfated curdlans by size exclusion chromatography (SEC). The results are summarized in Table 1. The M_w value suddenly dropped from 24,800 to 13,000 by introduction of 1.7 mol% sulfate group and then linearly decreased with increase in the DS. It is known that *p*-toluenesulfonic acid hydrolyzes the main chain of the β-(1→3)-glucan above 50 °C.[7,11] Taking into consideration that (i) pyridinium sulfate was generated during the sulfation and; (ii) the reaction was carried out at 80 °C, the drop in M_w by slight sulfation is quite reasonable. As mentioned above, the M_w's for the DS from 1.7 to 8.7 mol% are among the M_w range useful as a polynucleotide binder, whereas the M_w for CUR-S(76) is too low to bind poly(C). Accordingly, the subsequent discussions are mainly performed for the modified curdlans bearing the DS from 1.7 to 8.7 mol%.

† DS is too low to give a reliable value of S for elemental analysis.

2.2. Structural analysis of the sulfated curdlan

Uryu and coworkers reported that the reactivity of the OH groups in β-(1→3)-glucans with the sulfation reagent obeys the following order: 6-OH > 2-OH ≫ 4-OH.[12,15] On the other hand, our previous studies indicated that the 2-OH group in the β-(1→3)-glucan main chain plays important roles in the complex formation with polynucleotides.[5,6] Therefore, if a significant amount of sulfate groups is introduced at the O-2 group, the complexation ability should be diminished by the steric bulkiness of the sulfate group.

Nuclear magnetic resonance is a useful technique to determine the sulfated position in polysaccharides.[11,16] Assignment of the ^{13}C chemical shifts for the sulfated curdlan has already been reported by Uryu and coworkers.[16] When the OH groups are sulfated, the peaks (C-2′, C-4′, and C-6′) shift toward lower magnetic field by ca. 10 ppm.[16] We confirmed that in the ^{13}C NMR spectrum of CUR-S(76), only the C-6′ peak shifts to lower magnetic field. Therefore, we concluded that our modification took place at the C-6 hydroxyl group.

2.3. Water solubility of the sulfated curdlan samples

In order to estimate the water solubility after the sulfation, we measured the turbidity of the sulfated curdlan in water solution. The concentration of the sample was 0.77 mM based on the repeating glucose unit; this concentration is usually used in our complexation studies with polynucleotides. The change in the turbidity of the solution, which is induced by the precipitation and the intermolecular aggregation, was monitored by a change in the transmittance at 500 nm.

Table 1 summarizes the transmittance of the solutions. In the DS below 4.4 mol%, it was still difficult to dissolve curdlan in water completely; the sample solutions turned turbid after heating. On the other hand, when the DS increased up to 4.4 mol%, the samples dissolved well in water and the solutions were clear for at least 3 days. Furthermore, the sulfated curdlan samples with DS 8.7 and 76 mol% readily dissolved without

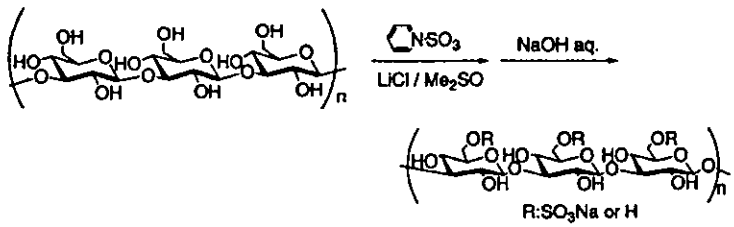

Scheme 1. Synthesis of the sulfated curdlan.

Table 1. Molecular mass data, DS, and transmittance of the sulfated curdlan

Sample code	M_n	M_w	M_w/M_n	DS (mol%) for the glucose unit[a]	Transmittance at 500 nm (%)
CUR-S(0)	18,000	24,800	1.38	0	59 (P)
CUR-S(1.7)	10,000	13,000	1.31	1.7 ± 0.2	73 (P)
CUR-S(2.2)	10,000	13,200	1.32	2.2 ± 0.3	69 (P)
CUR-S(4.4)	8500	12,200	1.44	4.4 ± 0.2	100 (S)
CUR-S(8.7)	8000	11,700	1.46	8.7 ± 0.3	100 (S)
CUR-S(76)	3100	5900	1.89	76 ± 1	100 (S[a])

P: precipitation, S: soluble, S[a]: soluble without heating.
[a]The DS was estimated by ICP analysis.

heating. It is worthy of note that introduction of only a few percent of sulfate groups changes the water solubility drastically.

2.4. Comparison of the complexation behaviors

When poly(C) is mixed with β-(1→3)-glucan polysaccharides, the circular dichroism (CD) spectra specifically change due to complex formation; the intensity at 275 nm is enhanced and a new band appears at around 242 nm.[4-6] The same spectral change was also observed for the 2-aminoethanol-modified SPG system,[17,18] indicating that the spectral changes are common among the complexes formed between β-(1→3)-glucan polysaccharides and poly(C).

Figure 2 compares the CD spectra at 5 °C for the sulfated curdlan sample, where [θ] is the molecular ellipticity. The CD spectra for the mixtures of poly(C) and the sulfated curdlan (except for CUR-S(76)) show the same spectral changes as mentioned above, although the increment in their CD intensity becomes smaller in the DS up to 4.4 mol%. This result suggests that these sulfated curdlans can also form complexes with poly(C). To get a better insight into the complexation ability, we compared the melting behaviors as shown in Figure 3. Although the CD spectra of the poly(C) complexes formed from CUR-S(0), CUR-S(1.7), and CUR-S(2.2) are the same at 5 °C (see Fig. 2), the melting temperatures (T_m) are slightly different; the T_m values decreased with an increase in the DS. When the DS further increased, CUR-S(4.4) and CUR-S(8.7) showed a decrement in T_m. On the other hand, the melting curvature of CUR-S(76) completely merged with that of poly(C) itself, indicating that no complex formation took place.

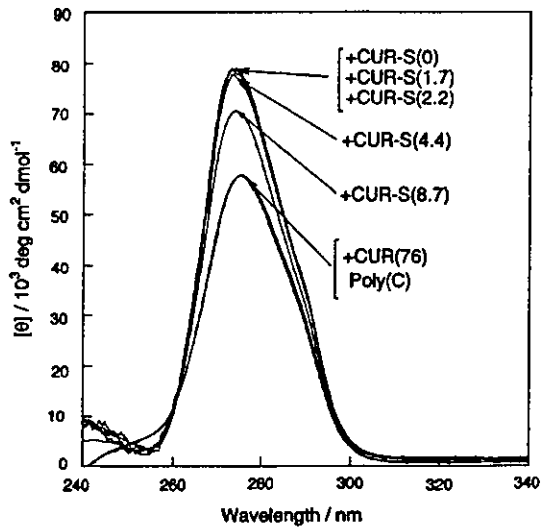

Figure 2. Comparison of the CD spectra at 5 °C for poly(C) and the sulfated curdlan samples.

Taking into consideration that (i) low-molecular-mass curdlans form complexes with poly(C) in the DS range from 1700 to 87,000 and; (ii) the modification does not take place at the C-2 hydroxyl group, it is likely that a high level of anion into curdlan inhibits the complexation. To estimate the modification effect quantitatively, we plotted the T_m values of the sulfated curdlan/poly(C) complex against their DS as shown in Figure 4. The T_m value decreases linearly with the increase in the DS indicating that the introduced sulfate groups destabilizes the complexes. Generally speaking, the electrostatic repulsion is much stronger in the nonsalt solutions; it is

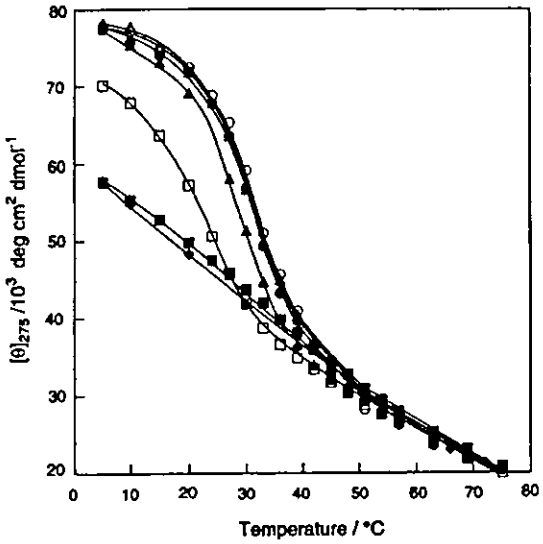

Figure 3. Comparison of the melting behaviors of the sulfated curdlan/poly(C) complexes. In the panel, poly(C) (◆), CUR-S(0)/poly(C) (○), CUR-S(1.7)/poly(C) (●), CUR-S(2.2)/poly(C) (△), CUR-S(4.4)/poly(C) (▲), CUR-S(8.7)/poly(C) (□), and CUR-S(76)/poly(C) (■), respectively.

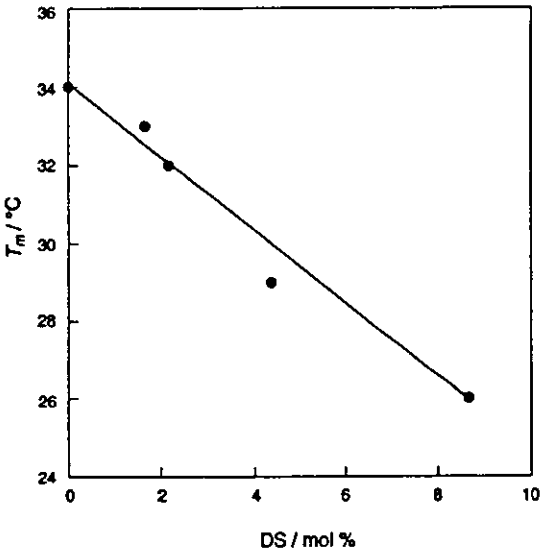

Figure 4. Relation between T_m of the complexes and their DS.

known that even DNA duplex cannot be formed in the nonsalt condition. Namely, the stability decrease shown in Figure 4 should be related to the electrostatic repulsion between the charges in the sulfate groups and poly(C) phosphate groups.

2.5. Salt concentration effect on the complex stability

To clarify whether the electrostatic repulsion destabilizes the complexes, we compared the T_m values from a relation between the thermal stability and the salt concentration. Since the electrostatic repulsion became smaller with the increase in the salt concentration, it is expected that the T_m could be enhanced with increasing NaCl concentration. Figure 5 shows the influence of the NaCl concentration on the T_m of the complexes formed between poly(C) and CUR-S(0), CUR-S(4.4), and CUR-S(8.7). In CUR-S(0), the increase in the NaCl concentration resulted in a maximum at around 50 mM similarly to the SPG/poly(C) system.[19] Although the T_m of CUR-S(4.4) was lower by 5 °C than that of CUR-S(0) at [NaCl] = 0 mM, the difference of T_m between CUR-S(0) and CUR-S(4.4) became smaller with an increase in the salt concentration and finally merged with that of CUR-S(0) at [NaCl] = 200 mM. The same phenomenon was also observed for CUR-S(8.7); the T_m increased with the concentration and merged with that of CUR-S(0) at [NaCl] = 200 mM. The results allow us to conclude that the electrostatic repulsion between the introduced sulfate group and the poly(C) phosphate group destabilizes the complex, but the effect becomes smaller with an increase in the salt concentration.

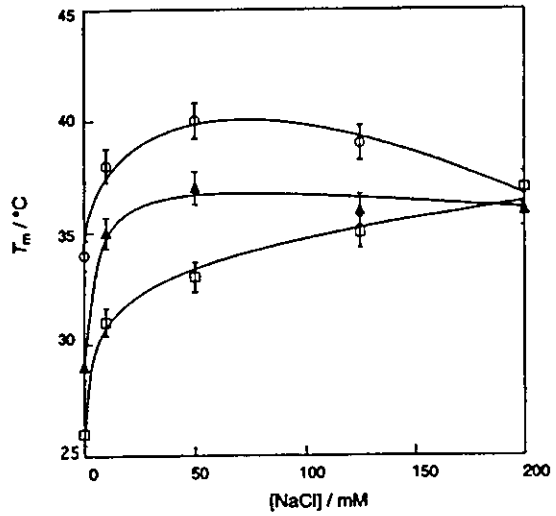

Figure 5. Salt concentration dependence of T_m. In the panel, CUR-S(0)/poly(C) (○), CUR-S(4.4)/poly(C) (▲), and CUR-S(8.7)/poly(C) (□), respectively.

By the way, when seeking to apply the sulfated curdlan to gene carrier problems, it is important to keep the salt concentration to some level and, furthermore, serum contains sodium chloride in the concentration range of 140–150 mM.[20] Such a high salt condition should suppress the electrostatic repulsion. Therefore, the stability decrease observed for the nonsalt condition should be inevitably negligible in serum; in other words, the present result supports the view that the partial sulfation is still a useful method in improving the water solubility without losing the complexation ability.

2.6. Resistance of the complexed polynucleotide chain against the enzymatic hydrolysis

To apply the sulfated curdlan/polynucleotide complex to gene carriers, we evaluated whether the complexed polynucleotide chain can resist the enzymatic hydrolysis.

The hydrolysis rate of the poly(C) chain bound to the sulfated curdlan by RNase A was evaluated as an increment of the absorbance at 260 nm according to the reported method,[21] which is ascribed to the production of cytidine-3′-monophosphate (CMP). In order to convert the absorbance at 260 nm to the CMP concentration, we used the following values for the extinction coefficient (ε): 9360 $cm^{-1} M^{-1}$ for CMP, 4850 $cm^{-1} M^{-1}$ for poly(C), 4530 $cm^{-1} M^{-1}$ for the CUR-S(4.4)/poly(C) complex, and 4560 $cm^{-1} M^{-1}$ for the CUR-S(8.7)/poly(C) complex, respectively. Figure 6 shows the CMP concentration versus incubation time plots at [NaCl] = 10 mM for poly(C), the CUR-S(4.4)/poly(C) complex, and CUR-S(8.7)/poly(C) complex. As can be seen, the complexation with the sulfated curdlan adequately suppressed the enzymatic hydrolysis although the protection effect was different between these two sulfated curdlan complexes. The hydrolysis rate constant was estimated from the initial slope in Figure 6 to be 4.7×10^{-9} M s^{-1} for poly(C), 8.1×10^{-10} M s^{-1} for the CUR-S(4.4)/poly(C) complex, and 1.3×10^{-9} M s^{-1} for the CUR-S(8.7)/poly(C) complex. The present hydrolysis reaction was carried out in [NaCl] = 10 mM. At this salt concentration, the thermal stability brought by the added salt is not so high (vide ante). Therefore, the conformational perturbation due to the electrostatic repulsion still remains in the complex and the perturbed segment should be easier to be hydrolyzed by RNase A.

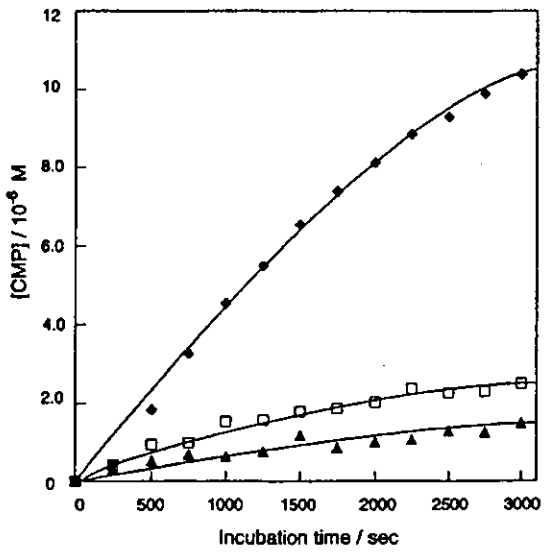

Figure 6. CMP concentration plotted against incubation time during hydrolysis by RNase A. In the panel, poly(C) (◆), CUR-S(4.4)/poly(C) (▲), and CUR-S(8.7)/poly(C) (□), respectively.

However, the hydrolysis rate of the sulfated curdlan complexes is still suppressed compared with that of the naked poly(C); the hydrolysis rate constants of the CUR-S(4.4)/poly(C) and CUR-S(8.7)/poly(C) complexes are smaller by one-sixth and one-fourth than that of poly(C), respectively. The present resistance effect against the enzymatic hydrolysis indicates that the sulfated curdlan can be well applicable to gene carriers.‡

3. Conclusion

Five sulfated curdlan samples with DS ranging from 0 to 76 mol% were prepared. The sulfated curdlan samples have improved water solubility. CD measurements revealed that those with DS from 1.7 to 8.7 mol% can form complexes with poly(C) as schizophyllan does. Although the thermal stability of the complex decreased by the introduction of sulfate groups due to electrostatic repulsion, it could be regained by salt addition. Furthermore, the complexed polynucleotide chain showed a significant resistance against enzymatic hydrolysis. Taking these results into consideration, we believe that curdlan could be used as functional material for gene technology.

4. Experimental

4.1. General

Curdlan was purchased from Wako Pure Chemical Industries, Ltd. (Osaka, Japan). Me_2SO with a spectroscopic grade and lithium chloride were purchased from Kishida Chemical Co., Ltd. (Osaka, Japan), poly(C) and ribonuclease A (RNase A, E.C.3.1.27.5) from Amersham (NJ, USA), and pyridine–sulfur trioxide complex from Aldrich (WI, USA). All reagents were used without further purification. An RNase free and sterile water was used for all measurements. Sample solutions were prepared according to our previous reports.[5,16]

4.2. Syntheses of the sulfated curdlan

Curdlan used in this study ($M_w = 24{,}800$, $M_w/M_n = 1.38$) was prepared by acid hydrolysis according to the reported method.[7] The curdlan (200 mg) was dissolved in Me_2SO (50 mL) in the presence of LiCl (0.25 M) and stirred at 80 °C overnight. The pyridine–sulfur trioxide

‡ We have confirmed that addition of CUR-S(76), which does not bind poly(C) but may interact with RNase A, scarcely changes the hydrolysis rate of poly(C). This means that in the present kinetic study the contribution of the sulfated curdlan–RNase A interaction is almost negligible.

complex was added to the solution while maintaining the temperature and stirred for 4 h under N_2. The reaction mixture was immediately cooled to room temperature and neutralized with 0.1 M aq. NaOH solution. The solution was dialyzed with distilled water for 1 week using a cellulose tube membrane ($M_w < 3500$ cut) and then lyophilized using an EYELA freeze dryer FD-5N. We thus obtained sulfated curdlan samples. To confirm the countercation, we carried out atomic absorption spectroscopy (Shimadzu AA-6700) for all samples and found that the molar concentration of sulfur determined by ICP is almost equal to that of sodium determined by atomic absorption spectroscopy. This coincidence indicates that the countercation of the sulfate group is sodium.

4.3. Determination of the content of the introduced sulfate group

The content of sulfate group was evaluated as the amount of sulfur% in the sample obtained from ICP analyses (Perkin Elmer Optima 3100RL). The calibration curve of sulfur was built using the sulfur oil standard solution (9949 ppm, ref. 44, 173-2 from Aldrich). The ICP analyses were carried out nine times for each sample and the average was used for the final value of the DS. The sample solutions for the ICP analysis were prepared as follows: the sulfated curdlan sample (2.0 mg) was dissolved in DMF (0.3 mL) and the mixture was diluted with distilled water (9.7 mL).

4.4. SEC analysis

The molecular mass was evaluated by SEC using a Tosoh HLC-8020; apparatus: two α-4000 columns are connected in series, LiBr (20 mM)/DMF was used as elution solvent, and the instrument was calibrated by a polyethyleneoxide standard (Tosoh Co., Japan).

4.5. Water-solubility test

The water solubility of the sulfated samples was estimated as a function of transmittance of the sulfated curdlan in water solution. The transmittance was recorded on a Shimadzu UV-2500 spectrometer with a 1 cm cell. The sample was prepared as follows: after dissolution of the curdlan sample (1.0 mg) in distilled water upon heating, the sample was cooled to room temperature, aged for 3 days, and then the transmittance was estimated at 500 nm.

4.6. ^{13}C NMR spectra

The NMR spectrum was recorded on a Bruker DRX600 spectrometer at 37 °C. A sample for the NMR measurements contained 70 mg of the curdlan sample dissolved in 0.75 mL of D_2O and 4,4-dimethyl-4-silapentane-1-sulfonate (DSS) was used as an internal standard. Assignment of each peak was confirmed using ^1H–^{13}C correlation spectroscopy (COSY).

4.7. Enzymatic hydrolysis of poly(C) chain

The increment of the CMP concentration arising from the hydrolysis of poly(C) chain by RNase A was monitored on a UV–vis spectrometer with a 1 cm cell (JASCO V-570UV/VIS/NIR spectrometer). The stoichiometric curdlan/poly(C) complex (six glucose units form complex with three cytosine residues), including Tris (pH 8.0), Me_2SO, and NaCl, was prepared and aged at 4 °C for at least 3 days. After the RNase A soln was added to the sample soln, the incubation was started at 10 °C. This temperature was chosen so as to be lower than the dissociation temperature of the corresponding complexes. The final concentrations were adjusted as follows: $V_w = 0.92$, where V_w is the water vol fraction in the Me_2SO water mixture, [poly(C)] = 0.10 mM/repeating unit, [curdlan] = 0.24 mM/repeating glucose unit, [Tris] = 0.8 mM, [NaCl] = 50 mM, and [RNase A] = 2.0×10^{-4} g L^{-1}.

Acknowledgements

We thank Taito Co., Japan for providing the schizophyllan samples. K.K. is indebted to the Japan Society for the Promotion of Science (JSPS) for financial support. This research has been conducted under the financial support from the JST SORST Program.

References

1. Part 13: Mizu, M.; Koumoto, K.; Kimura, T.; Sakurai, K.; Nagasaki, T.; Shinkai, S. *J. Controlled Release*, in press.
2. *Biopolymers, Vol. 5: Polysaccharides I—Polysaccharide from Prokaryotes*; Vandamme, E. J., De Baets, S., Steinbüchel, A., Eds.; Wiley-VCH: Weinheim, 2002.
3. *Biopolymers, Vol. 6: Polysaccharides II—Polysaccharide from Eukaryotes*; Vandamme, E. J., De Baets, S., Steinbüchel, A., Eds.; Wiley-VCH: Weinheim, 2002.
4. Sakurai, K.; Shinkai, S. *J. Am. Chem. Soc.* **2000**, *122*, 4520–4521.
5. Sakurai, K.; Mizu, M.; Shinkai, S. *Biomacromolecules* **2001**, *2*, 641–650.
6. Kimura, T.; Koumoto, K.; Sakurai, K.; Shinkai, S. *Chem. Lett.* **2000**, 1242–1243.
7. Koumoto, K.; Kimura, T.; Kobayashi, H.; Sakurai, K.; Shinkai, S. *Chem. Lett.* **2001**, 908–909.
8. Sakurai, K.; Iguchi, R.; Kimura, T.; Koumoto, K.; Mizu, M.; Shinkai, S. *Polym. Prepr. Jpn.* **2000**, *49*, 4054.
9. Sakurai, K.; Shinkai, S.; Koumoto, K. *Polym. Prepr.* **2002**, *43*, 691.
10. Kobayashi, R.; Sakurai, K.; Kimura, T.; Koumoto, K.; Mizu, M.; Shinkai, S. *Polym. Prepr. Jpn.* **2001**, *50*, 4054.